Coupled-channels study of the $\pi^- p \to \eta n$ process

J. Durand,[1] B. Juliá-Díaz,[2,3] T.-S. H. Lee,[3,4] B. Saghai,[1] and T. Sato[5,3]

[1] *Institut de Recherche sur les lois Fondamentales de l'Univers,*

DSM/IRFU, CEA/Saclay, 91191 Gif-sur-Yvette, France

[2] *Facultat de Fisica, Universitat de Barcelona, E-08028 Barcelona, Spain*

[3] *Excited Baryon Analysis Center (EBAC),*

Thomas Jefferson National Accelerator Facility, Newport News, VA 22901, USA

[4] *Physics Division, Argonne National Laboratory, Argonne, IL 60439, USA*

[5]*Department of Physics, Osaka University, Toyonaka, Osaka 560-0043, Japan*

(Dated: April 22, 2008)

Abstract

The reaction $\pi^- p \to \eta n$ is investigated within a dynamical coupled-channels model of meson production reactions in the nucleon resonance region. The meson baryon channels included are πN, ηN, $\pi\Delta$, σN, and ρN. The non-resonant meson-baryon interactions of the model are derived from a set of Lagrangians by using a unitary transformation method. One or two excited nucleon states in each of S, P, D, and F partial waves are included to generate the resonant amplitudes. Data of $\pi^- p \to \eta n$ reaction from threshold up to a total center-of-mass energy of about 2 GeV are satisfactorily reproduced and the roles played by the following nine nucleon resonances are investigated: $S_{11}(1535)$, $S_{11}(1650)$, $P_{11}(1440)$, $P_{11}(1710)$, $P_{13}(1720)$, $D_{13}(1520)$, $D_{13}(1700)$, $D_{15}(1675)$, and $F_{15}(1680)$. The reaction mechanism as well as the predicted ηN scattering length are discussed.

PACS numbers: 11.80.-m, 11.80Gw, 13.75.-n, 24.10.Eq

I. INTRODUCTION

In spite of the quasi extinction of pion beams facilities since about two decades, we are witnessing a growing interest in theoretical investigations of pion $-$ nucleon (πN) interactions. This is mainly due to the well recognized fact [1, 2] that the impressive amount of high quality data on electromagnetic meson production reactions from several facilities (ELSA, GRAAL, JLab, LEPS, and MAMI) can be used to pin down the underlying reaction mechanisms and to study the role and/or properties of intervening baryon resonances only when the corresponding hadronic production reactions can also be consistently understood. The present work is a prelude to a comprehensive study of the process $\gamma p \rightarrow \eta p$, where, regardless of the direct production mechanisms considered, a meaningful determination of the resonances properties from the η photoproduction data requires the inclusion of intermediate and final state meson-nucleon interactions. This latter task is tackled to in the present work by analyzing the world data of $\pi^- p \rightarrow \eta n$ reaction.

To see the main features of our approach, it is useful to briefly describe here some of the recent theoretical works which account for the data of $\pi^- p \rightarrow \eta n$ reaction. The K-matrix coupled-channels approach by Sauermann *et al.* [3], included only πN and ηN channels and was limited to the S_{11} partial wave. Such a K-matrix approach was then extended by Green and Wycech [4] to include the γN channel in a combined analysis of both $\pi^- p \rightarrow \eta n$ and $\gamma p \rightarrow \eta p$ reactions, and more extensively developed by the Giessen Group [5–7] to include πN, ηN, $2\pi N$, ωN, $K\Lambda$, and $K\Sigma$ channels. The approach developed by the Bonn Group [8, 9] is also a K-matrix coupled-channels model supplemented with Regge phenomenology. The approach taken by the Zagreb Group [10–13] has concentrated on performing the partial-wave analysis of $\pi N \rightarrow \pi N$, ηN reactions data. This latter approach is most extensively developed by the Virginia Polytechnic Institute - George Washington University (SAID) Group [14], and is regularly updated.

In this work, we start with a dynamical coupled-channels model which is based on a Hamiltonian formulation [2] and was applied [15] to analyze πN elastic scattering data. This theoretical framework, embodying the πN, ηN, $\pi\Delta$, σN, and ρN channels, is an extension of the approach of Ref. [16] and is rather different from the K-matrix models described above, as discussed in detail in Refs. [2, 15]. Qualitatively speaking, the K-matrix approaches, which can be derived [1] from a dynamical formulation by taking the on-shell

approximation, avoid an explicit treatment of the reaction mechanisms in the short range region, where we want to map out the quark-gluon substructure of the excited states (N^*) of the nucleon. Such a simplification in interpreting the data is also not taken in other dynamical approaches such as those developed recently in Refs. [17–19] and the earlier works reviewed in Ref. [1]. Besides the approaches mentioned above, attempts [20, 21] to introduce subnucleonic degrees of freedom in studying $\pi^- p \to \eta n$ reaction are also becoming available.

Moreover, combining the dynamical coupled-channels approach and the constituent quark model approach [22] to study [23–25] $\gamma p \to K^+ \Lambda$ process proves to be a useful step in deepening our understanding of the baryon spectroscopy and search for missing nucleon resonances [26].

This work follows closely the model (JLMS) developed [15] in a study of πN elastic scattering. The relevant scattering equations are be described in Section II. Section III is devoted to model building procedure and evaluation of the data base. In the same Section, we present our results for differential and total cross-sections of the process $\pi^- p \to \eta n$, in the center-of-mass energy range $W \lesssim 2$ GeV, and discuss the main features of the considered reaction mechanism. In Section IV the ingredients of the constructed model are used to predict the ηN scattering length, as well as the total cross-section for the process $\eta p \to \eta p$. Summary and conclusions are reported in Section V.

II. THEORETICAL FRAMEWORK

A detailed description of the coupled-channels formalism can be found in Refs. [2, 15]. We outline here the main ingredients which are necessary to understand the procedure followed in the present work.

The meson baryon (MB) transition amplitudes in each partial wave can be written as,

$$T_{MB,M'B'}(E) = t^{NR}_{MB,M'B'}(E) + t^{R}_{MB,M'B'}(E),$$ (1)

where,

$$MB \equiv \pi N, \ \eta N, \ \pi \Delta, \ \rho N, \ \sigma N.$$ (2)

The full amplitudes $T_{MB,M'B'}(E)$ can be directly used to calculate $MB \to M'B'$ scattering

observables. The non-resonant amplitude $t^{NR}_{MB,M'B'}(E)$ in Eq. (1) is defined by the coupled-channels equations,

$$t^{NR}_{MB,M'B'}(E) = V_{MB,M'B'}(E) + \sum_{M''B''} V_{MB,M''B''}(E)\, G_{M''B''}(E)\, t^{NR}_{M''B'',M'B'}(E)\,, \qquad (3)$$

with $G_{M''B''}(E)$ meson-baryon propagators, and,

$$V_{MB,M'B'}(E) = v_{MB,M'B'} + Z^{(E)}_{MB,M'B'}(E)\,. \qquad (4)$$

The interactions $v_{MB,M'B'}$ are derived from tree-level processes by using a unitary transformation method. They are energy independent and free of singularities. On the other hand, $Z^{(E)}_{MB,M'B'}(E)$ is induced by the decays of the unstable particles (Δ, ρ, σ) and thus contains *moving* singularities due to the $\pi\pi N$ cuts. As emphasized in Ref. [15], we neglect that term at this stage.

The second term in the right-hand-side of Eq. (1) is the resonant term defined by

$$t^{R}_{MB,M'B'}(E) = \sum_{N^*_i,N^*_j} \bar{\Gamma}_{MB\to N^*_i}(E)[D(E)]_{i,j}\bar{\Gamma}_{N^*_j\to M'B'}(E)\,, \qquad (5)$$

with the N^* propagator,

$$[D^{-1}(E)]_{i,j} = (E - M^0_{N^*_i})\delta_{i,j} - \bar{\Sigma}_{i,j}(E)\,, \qquad (6)$$

where $M^0_{N^*}$ is the bare mass of the resonant state N^*, and the self-energies are,

$$\bar{\Sigma}_{i,j}(E) = \sum_{MB} \Gamma_{N^*_i\to MB} G_{MB}(E)\bar{\Gamma}_{MB\to N^*_j}(E)\,. \qquad (7)$$

The dressed vertex interactions in Eq. (5) and Eq. (7) are (defining $\Gamma_{MB\to N^*} = \Gamma^{\dagger}_{N^*\to MB}$),

$$\bar{\Gamma}_{MB\to N^*}(E) = \Gamma_{MB\to N^*} + \sum_{M'B'} t^{NR}_{MB,M'B'}(E)G_{M'B'}(E)\Gamma_{M'B'\to N^*}\,, \qquad (8)$$

$$\bar{\Gamma}_{N^*\to MB}(E) = \Gamma_{N^*\to MB} + \sum_{M'B'} \Gamma_{N^*\to M'B'}G_{M'B'}(E)t^{NR}_{M'B',MB}(E)\,. \qquad (9)$$

The parameterization used for $\Gamma_{N^*,MB}$ is explained in Ref. [15].

The meson-baryon propagators G_{MB} in the above equations are,

$$G_{MB}(k,E) = \frac{1}{E - E_M(k) - E_B(k) + i\epsilon}, \qquad (10)$$

for the stable particle channels $MB \equiv \pi N,\ \eta N$, and,

$$G_{MB}(k,E) = \frac{1}{E - E_M(k) - E_B(k) - \Sigma_{MB}(k,E)}, \qquad (11)$$

for the unstable particle channels $MB \equiv \pi\Delta$, ρN, σN. The self-energies in Eq. (11) are computed explicitly as defined in Ref. [15].

To solve the coupled-channels equations, Eq. (3), we need to regularize the matrix elements of $v_{MB,M'B'}$. We include at each meson-baryon-baryon vertex a form factor of the following form:

$$F(\vec{k}, \Lambda) = \left[\frac{\vec{k}^2}{\vec{k}^2 + \Lambda^2} \right]^2, \tag{12}$$

with $\vec{k}$ being the meson momentum. For the meson-meson-meson vertex of v^t, the form factor in Eq. (12) is also used with $\vec{k}$ being the momentum of the exchanged meson. For the contact term v^c, we regularize it by $F(\vec{k}, \Lambda)F(\vec{k}', \Lambda')$. Here we follow Ref. [15] and use the parameter values determined there for all non-resonant terms except the ones explicitly mentioned in the following Sections.

With the non-resonant amplitudes generated from solving Eq. (3), the resonant amplitude $t^R_{MB,M'B'}$ in Eq. (5) then depends on the bare mass $M^0_{N^*}$ and the bare $N^* \to MB$ vertex functions. The vertex functions are parameterized in the following way,

$$\Gamma_{N^*,MB(LS)}(k) = \frac{1}{(2\pi)^{3/2}} \frac{1}{\sqrt{m_N}} C_{N^*,MB(LS)} \left[\frac{\Lambda^2_{N^*,MB(LS)}}{\Lambda^2_{N^*,MB(LS)} + (k - k_R)^2} \right]^{(2+L)} \left[\frac{k}{m_\pi} \right]^L. \tag{13}$$

where L and S are the orbital angular momentum and the total spin of the MB system, respectively. $C_{N^*,MB(LS)}$ measure the meson-nucleon-N^* coupling strength for a specific LS combination of the MB system and are taken as free parameters, and k_R are parameters fixed by the $\pi N \to \pi N$ analysis in Ref. [15]. The above parameterization accounts for the threshold k^L dependence and the right power $(2+L)$ such that the integration for calculating the dressed vertex Eqs. (8) and (9) is finite.

III. RESULTS AND DISCUSSION

The world data base for the process under investigation embodies 1508 differential and 98 total cross-sections [27–35] for $1.47 \leq W \leq 2.85$ GeV. However, those data presented in 12 papers, thesis, and reports have been obtained mainly between 1964 and 1980, except for recent results from the Brookhaven National Laboratory and using the Crystal Ball detector by Morrison [27] and Prakhov *et al.* [28]. The quality of data obtained before 1980 has been discussed by Clajus and Nefkens [36] and emphasized by George Washington University [14],

Zagreb [10] and Giessen [6, 7] Groups, underlying inconsistencies among different data sets, because of experimental shortcomings and the underestimate of systematic uncertainties. This uncomfortable situation has leaded various authors to use a reduced data base. For example, the GWU Group [14] includes in the data base 257 data points, mainly from differential cross-section measurements [27–30], but also about 50 data points for total cross-sections [27, 29, 30, 33, 35].

In the present work, we concentrate only on the differential cross-sections for $W \lesssim 2$ GeV, as summarized in Table I. The number of data points included in the fitted data base in this work (294) will be discussed in Sec. III A.

One of the delicate points in dealing with those data is related to the systematic uncertainties (δ_{sys}). For the most recent data by Prakhov *et al.* [28] those uncertainties are given clearly by the authors (6%). For old data, we have mainly followed the general trend suggested in Ref. [36], as summarized in the last column of Table I. Deinet *et al.* [29] report two sources of systematic uncertainty: 7% and 9%, to be added up quadratically, giving $\delta_{sys} = 11.4\%$. For Richards *et al.* [30], we have used $\delta_{sys} = 10\%$ for the lowest energies, 11% to 14% for other ones, as given in the original paper. For Debenham *et al.* [31] and Brown *et al.* [32], we have followed the conclusion of the Zagreb Group [10, 12]. In the case of Brown *et al.* [32], we also have lowered the momentum by 4%, in lines with Ref. [36].

Total cross-section data has not been included in our fits due to the following reasons: i) differential cross-sections are measured by various collaborations in significantly different angular ranges with respect to extreme ones (see second column in Table I), ii) there is no commonly agreed upon procedure to extract total cross-sections from measured angular distributions, iii) model predictions for extreme angles do not in general agree with each other.

A. Fitting procedure

As mentioned above, in Ref. [15] the $\pi N \to \pi N$ reaction was studied within a coupled-channels formalism, with multi-step processes embodying πN, ηN, $\pi \Delta$, σN, and ρN states.

In that work 175 adjustable parameters were introduced to fit amplitudes produced by the SAID Group, fitting more than 10000 data points. About 30 of those parameters are particularly relevant to the coupled-channels mechanisms for the $\pi^- p \to \eta n$ reaction. Ac-

Ref.	Angular range	P_π	W	N_{dp}	N_{dp} used in the	δ_{sys}
	(Degrees)	(GeV/c)	(GeV)		the present work	
Prakhov et al. [28]	23 - 157	0.687 - 0.747	1.49 - 1.52	84	70	6%
Deinet et al. [29]	32 - 123	0.718 - 1.050	1.51 - 1.70	83	80	11%
Richards et al. [30]	26 - 154	0.718 - 1.433	1.51 - 1.90	70	66	10% to 14%
Debenham et al. [31]	162 - 172	0.697 - 0.999	1.49 - 1.67	111	27	10% + 0.02 mb
Brown et al. [32]	18 - 160	0.724 - 2.724	1.51 - 2.45	379	51	10% or 0.01 mb
Morrison [27]	46 - 134	0.701 - 0.747	1.50 - 1.52	34	-	
Crouch et al. [33]	14 - 167	1.395 - 3.839	1.88 - 2.85	731	-	
Feltesse et al. [34]	20 - 160	0.757	1.53	16	-	

TABLE I: Summary of differential cross-section data for the reaction $\pi^- p \to \eta n$. Data sets investigated in the present work are singled out in the last two columns, where the number of data points (N_{dp}) per data set used in the fitting procedure is given.

cordingly, in the present work we use that reduced set of adjustable parameters (see Table II) and fix the others to their values as determined in Ref. [15] (cf. Tables III to VII in that paper). A total of 294 data points are fitted in the present work (see Table I). Here, we wish to make a comment on the exclusion of a few data points in Ref. [28] from the fitted data-base. Actually, as mentioned above, on the one hand, recent data by Prakhov et al. [28] bear much smaller errors than other data, and on the other hand, the data-base suffers from some inconsistencies. One of the consequences of this situation is that a few data points introduce large χ^2s (around 10 or more) thus reducing significantly the efficiency of the minimization procedure. The excluded points concern mainly the two lowest energy sets of Ref. [28].

In the following we present our results for two models, as well as those obtained using the parameters reported in Ref. [15] (see Table II and Figs. 1-2).

Here, in lines with Ref. [15], the following nucleon resonances (N^*) are considered: $S_{11}(1535)$, $S_{11}(1650)$, $P_{11}(1440)$, $P_{11}(1710)$, $P_{13}(1720)$, $D_{13}(1520)$, $D_{13}(1700)$, $D_{15}(1675)$, and $F_{15}(1680)$.

The adjustable parameters for non-resonant terms are the ηNN coupling constant $f_{\eta NN}$ and cut-off $\Lambda_{\eta NN}$. For resonant terms the parameters are as follows: N^*s bare-masses $M_0^{N^*}$,

ηNN^* coupling strengths $C_{\eta NN^*}$, and cut-offs $\Lambda_{\eta NN^*}$.

Category	Parameter	Model A	Model B	Ref. [15]
Non-resonant ηN parameters:				
	$f_{\eta NN}$	4.9936	4.9999	3.8892
	$\Lambda_{\eta NN}$	592.11	591.91	623.56
Bare mass $M_0^{N^*}$:				
	$S_{11}(1535)$	1809	1808	1800
	$S_{11}(1650)$	1901	1861	1880
	$P_{11}(1440)$	1775	1784	1763
	$P_{11}(1710)$	2019	2057	2037
	$P_{13}(1720)$	1726	1691	1711
	$D_{13}(1520)$	1918	1919	1899
	$D_{13}(1700)$	1971	1968	1988
	$D_{15}(1675)$	1878	1878	1898
	$F_{15}(1680)$	2207	2207	2187
$C_{N^* \to MB(LS)}$:				
	$C_{\eta NS_{11}(1535)}$	8.4269	7.8344	9.1000
	$C_{\rho NS_{11}(1535)}$	*2.0280*	-0.4935	2.028
	$C_{\eta NS_{11}(1650)}$	2.0487	-0.4221	0.6000
	$C_{\rho NS_{11}(1650)}$	*-9.5179*	2.0000	-9.5179
	$C_{\eta NP_{11}(1440)}$	1.6321	1.6298	2.6210
	$C_{\eta NP_{11}(1710)}$	2.4925	2.4994	3.6611
	$C_{\eta NP_{13}(1720)}$	2.4474	2.4997	-0.9992
	$C_{\eta ND_{13}(1520)}$	0.4440	0.4267	-0.0174
	$C_{\eta ND_{13}(1700)}$	-1.8985	-0.6463	0.3570
	$C_{\eta ND_{15}(1675)}$	0.2456	0.3437	-0.0959
	$C_{\eta NF_{15}(1680)}$	-0.0446	-0.0265	0.0000
$\Lambda_{N^* \to MB(LS)}$:				
	$\Lambda_{\eta NS_{11}(1535)}$	779.38	799.90	598.97
	$\Lambda_{\rho NS_{11}(1535)}$	*1999.8*	670.89	1999.8
		1893.8	955.8	1893.8
	$\Lambda_{\eta NS_{11}(1650)}$	500.07	1999.70	500.02
	$\Lambda_{\rho NS_{11}(1650)}$	*796.83*	2000.00	796.83
	$\Lambda_{\eta NP_{11}(1440)}$	1766.80	1757.40	1654.85
	$\Lambda_{\eta NP_{11}(1710)}$	500.08	500.00	897.84
	$\Lambda_{\eta NP_{13}(1720)}$	631.90	649.11	500.23
	$\Lambda_{\eta ND_{13}(1520)}$	500.20	500.01	1918.20
	$\Lambda_{\eta ND_{13}(1700)}$	540.55	763.13	678.41
	$\Lambda_{\eta ND_{15}(1675)}$	507.64	500.00	1554.00
	$\Lambda_{\eta NF_{15}(1680)}$	811.72	1073.80	655.87
χ^2_{dp}		2.03	1.94	6.94

TABLE II: Parameters for models A and B determined in this work. The last column gives the values determined in Ref. [15].

Model A is obtained by fitting the data base and those 29 adjustable parameters (see column 3 in Table II). Model B, for reasons explained below, has five more adjustable parameters, namely, the coupling constants and cut-offs of ρNS_{11}, with $S_{11} \equiv S_{11}(1535)$ and $S_{11}(1650)$ for [LS] = [0, 1/2], as well as the cut off $\Lambda_{\rho NS_{11}(1535)}$ for [LS] = [2, 3/2]. Finally, for comparisons, we reproduce in Table II the relevant values reported in Ref. [15]. As mentioned above, in that latter work, adjustable parameters are determined *via* the $\pi N \rightarrow \pi N$ channels, and for the $\pi^- p \rightarrow \eta n$ the data base embodied only a few total cross-section data from Refs. [28, 32]. Notice that the five ρNS_{11} parameters in model A (shown in italics in Table II) were not treated as adjustable parameters, and hence, are identical to those of Ref. [15].

B.   Differential and total cross-sections for the process $\pi^- p \rightarrow \eta n$

In Figures 1 and 2 we compare the results of the models A and B with the differential cross-section data, for which the reduced χ^2s per data point are 2.03 and 1.94, respectively. Those numbers compare well with the GWU [14] reduced $\chi^2 = 2.44$. In the same figures, we also show results obtained by using the parameters of Ref. [15], which gives $\chi^2 = 6.94$.

Before discussing different curves in comparison with data, we wish to emphasize the difference between models A and B. Once the model A obtained, we investigated the importance of various parameters and found that by switching off the ρ coupling to the $S_{11}(1535)$, the χ^2 increases by roughly a factor of 3. Within the investigated reaction, such a high sensitivity to the ρNS_{11} seems unrealistic. To cure that behavior, we refitted the data by allowing those coupling constants to vary in the range of ± 0.5 for $S_{11}(1535)$ and ± 2 for $S_{11}(1650)$, instead of ± 10. The model B is then obtained, where that effect is significantly reduced. Comparing the two models in Figs. 1 and 2, we observe that they differ from each other by less than the statistic uncertainties of the data, corroborating that the $\pi^- p \rightarrow \eta n$ reaction is not a proper channel to pin down those couplings. Better constraints on those couplings can be obtained by investigating the $\pi N \rightarrow \pi \pi N$ process [37].

Models A and B show reasonable agreements with Prakhov *et al.* [28] data, except at the lowest energy (Fig. 1). We will come back to that point later. At four common energies, data from Morrison [27] are also depicted. That latter data set, not included in our fitting procedure, shows systematically smaller cross-sections compared to Ref. [28] data.
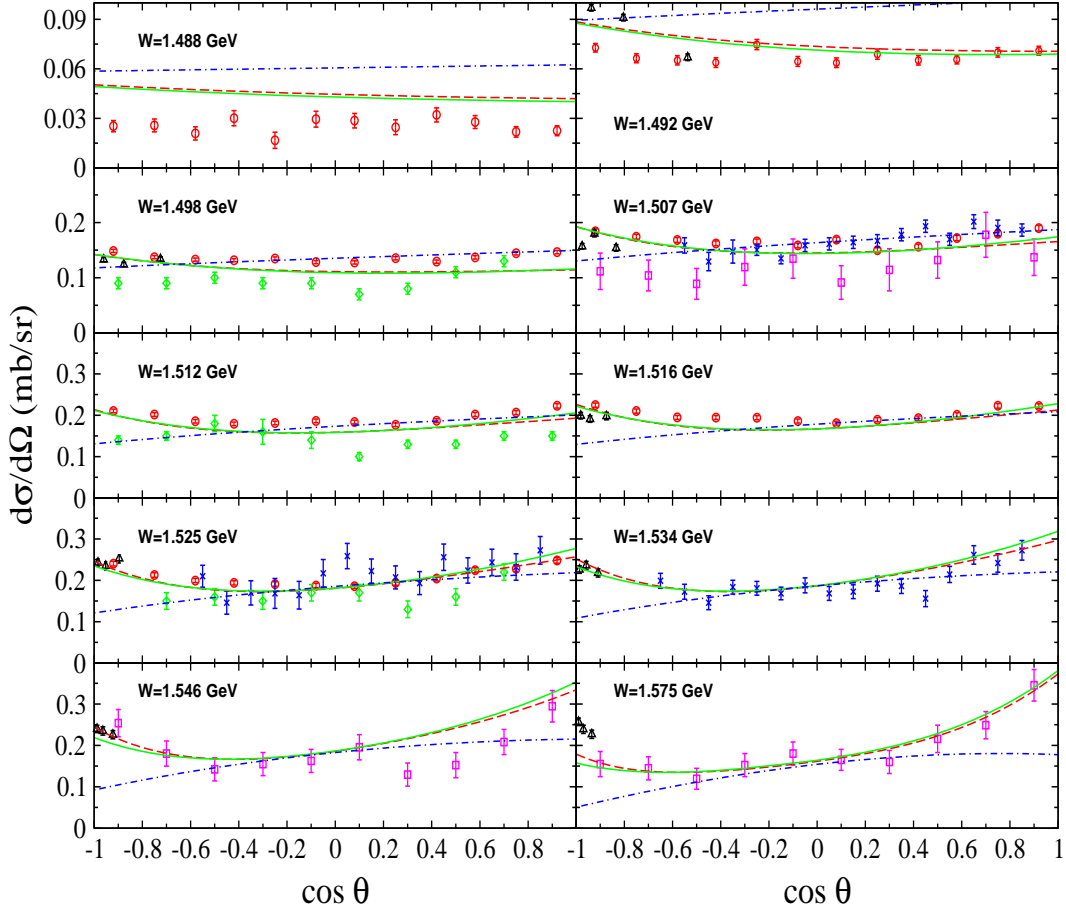
9

FIG. 1: Differential cross-section for the reaction $\pi^- p \to \eta n$. The curves correspond to models A (dashed) and B (full) from the present work. The dash-dotted curves are obtained by using the parameters in Ref. [15]. Data are from Prakhov *et al.* [28] (empty circles), Deinet *et al.* [29] (cross), Richards *et al.* [30] (empty squares), Debenham *et al.* [31] (up-triangles), and Morrison [27] (diamonds). Data uncertainties depicted are only statistic ones.

Prakhov *et al.* [28] data set at $W = 1.507$ GeV is of special interest, since there are also data from three other measurements. Results from Deinet *et al.* [29] are compatible with Prakhov *et al.* data, though with larger uncertainties (which become even more sizeable at $W = 1.525$ GeV). Richards *et al.* [30] data show deviations from Prakhov *et al.* ones, especially at most backward angles. Finally, copious data from Debenham *et al.* [31] are unfortunately limited to extreme backward angles and appear to be rather consistent with
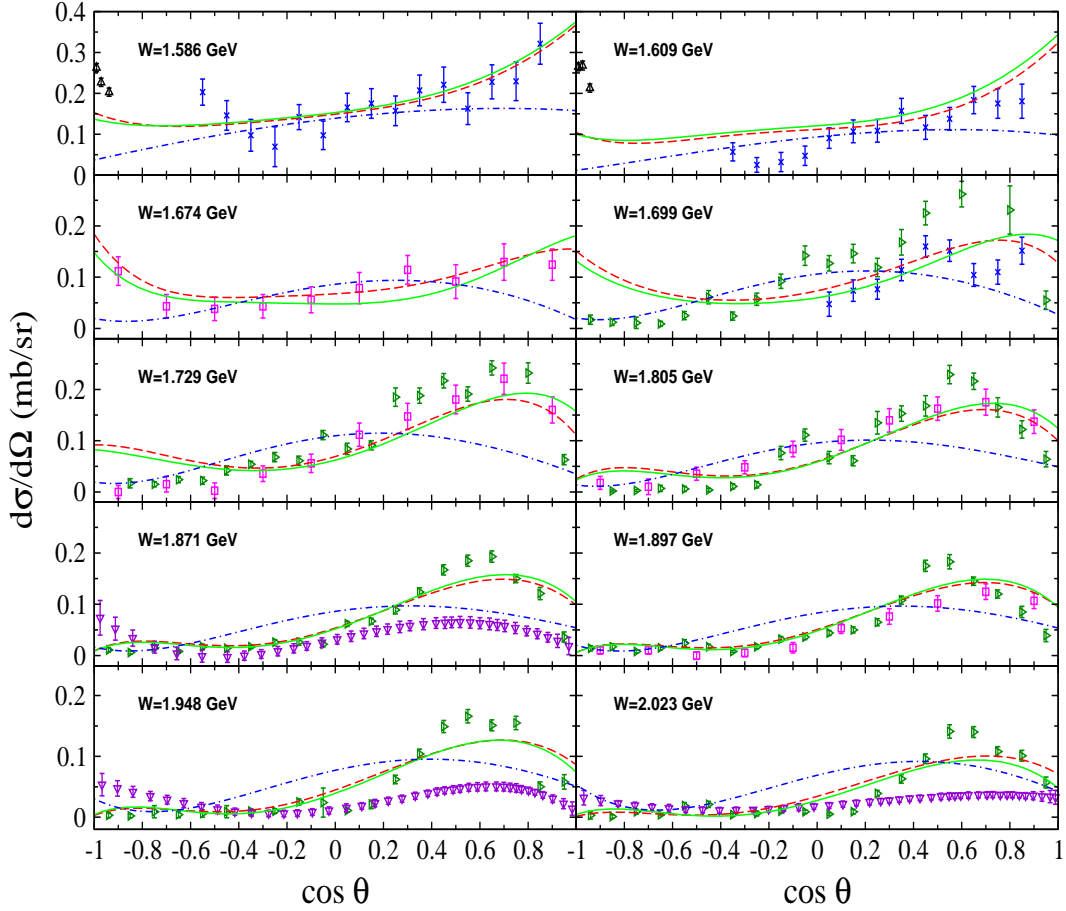
FIG. 2: Differential cross-section for the reaction $\pi^- p \to \eta n$. Curves and data as in Fig. 1 . Additional data are from Brown *et al.* [32] (right-triangles) and Crouch *et al.* [33] (down-triangles).

other data only up to $W \approx 1.55$ GeV. This trend is confirmed in Fig. 2, where models A and B reproduce correctly results from Deinet *et al.* [29] and Richards *et al.* [30]. Both sets of data come out fairly compatible with measurement from Brown *et al.* [32] at $W = 1.699$, 1.729, and 1.805 GeV. Models A and B show acceptable agreements with those data, except at backward angles, where the model / experiment discrepancies get reduced when energy increases and suitable agreement is observed at $W = 1.897$ GeV. At the three remaining depicted energies ($W = 1.871$, 1.948, and 2.003 GeV) our models reproduce the general trend of Brown *et al.* data. At those energies, data from Crouch *et al.* [33], not included in our data base, are also shown. The two data sets are not consistent. Given the known problems [36] with Brown's data, we made also attempts to fit the data base, within model

11

A, by replacing the Brown *et al.* data by those of Crouch *et al.* at $W = 1.879$ and 1.915 GeV. However, we observed a significant increase of χ^2 which goes from 2.03 to 4.12, and with very undesirable effects in the Crystal Ball energy range.
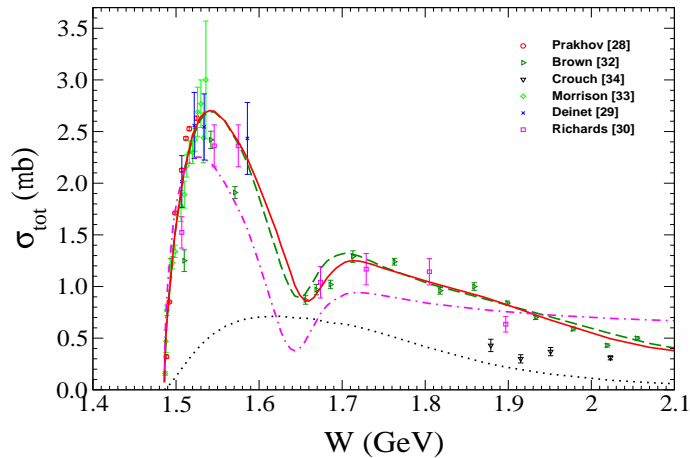

FIG. 3: Total cross-section for the reaction $\pi^- p \to \eta n$. Curves are from Ref. [15] (dash-dotted), model *A* (dashed), model *B* (full), and the background contributions (dotted) in model *B*. Data are as in Figs. 1 and 2.

In Figures 1 and 2, results using the parameters in Ref. [15] are also shown. At lowest energies, that model overestimates the data. At higher energies, it shows significant deviations, first at backward angles and then at forward angles. Above $W \approx 1.8$ GeV it tends to miss the data.

Finally, as mentioned above, we did not include the extracted total cross-section data in our data-base. In Fig. 3, we show the postdictions of our models *A* and *B*, as well as results of the Ref. [15], and compare them with the data. Both models *A* and *B* reproduce correctly the data, except for those by Crouch *et al.* [33], for which the differential cross-sections turn out to be significantly smaller than other data, as shown in Fig. 2. Moreover, the background contributions show a smooth behavior and are small with respect to the full model results, except around the minimum of the total cross-section, where resonant terms produce highly destructive interferences.

To end this Section, we wish to emphasize that the results of Ref. [15] are extended to the process $\pi^- p \to \eta n$ and two models are obtained, reproducing equally well the general
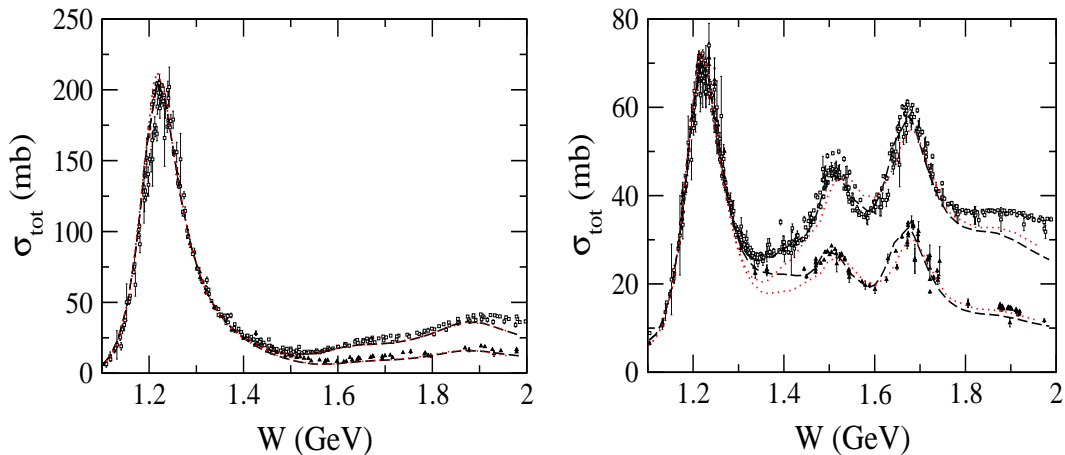
FIG. 4: Comparisons between the results from Ref. [15] (dashed curves) and from the model B (dotted curves) for $\pi N \rightarrow X, \pi N$ processes. Left panel: Predicted total cross-section for the reactions $\pi^+ p \rightarrow X$ (upper set) and $\pi^+ p \rightarrow \pi^+ p$ (lower set). Right panel: predicted total cross-section for the reactions $\pi^- p \rightarrow X$ (upper set) $\pi^- p \rightarrow \pi^- p + \pi^\circ n$ (lower set); Data in both panels are from Refs. [38, 39].

features of a heterogeneous data-base. This new set of parameters, particularly relevant to the investigated process, does not spoil the excellent results obtained in Ref. [15], and devoted mainly to the $\pi N \rightarrow \pi N$ observables. In order to illustrate this latter point, results from Ref. [15] and our model B are shown in Fig. 4, where Figs. [13] and [14] of Ref. [15] have been complemented with the predictions of the model B. For the processes with $\pi^+ p$ initial state (left panel in Fig. 4), results from the two models overlap with each other. For reactions involving $\pi^- p$ initial states (right panel in Fig. 4), model B gives deeper minima around $W \approx 1.4$ GeV than those reported in Ref. [15], with the largest discrepancy between the two curves being less than 20%. Comparing the partial-wave amplitudes of those models, the main differences appear in the P_{11}- and P_{13}-waves.

C. Main features of the $\pi^- p \rightarrow \eta n$ reaction mechanism

In order to shed insights to the main ingredients of the reaction mechanism, we concentrate on model B. Starting from that model, and without further minimizations, we have

checked the variations of the χ^2 by switching off the nine resonances one by one. The results are reported in Table III.

	$S_{11}(1535)$	$S_{11}(1650)$	$P_{11}(1440)$	$P_{11}(1710)$	$P_{13}(1720)$	$D_{13}(1520)$	$D_{13}(1700)$	$D_{15}(1675)$	$F_{15}(1680)$
χ^2	48.86	2.62	3.55	2.37	2.77	2.23	1.93	2.10	2.47

TABLE III: Reduced χ^2 per data point for model B with one resonance switched off (the reduced χ^2 for the full model B being 1.94).
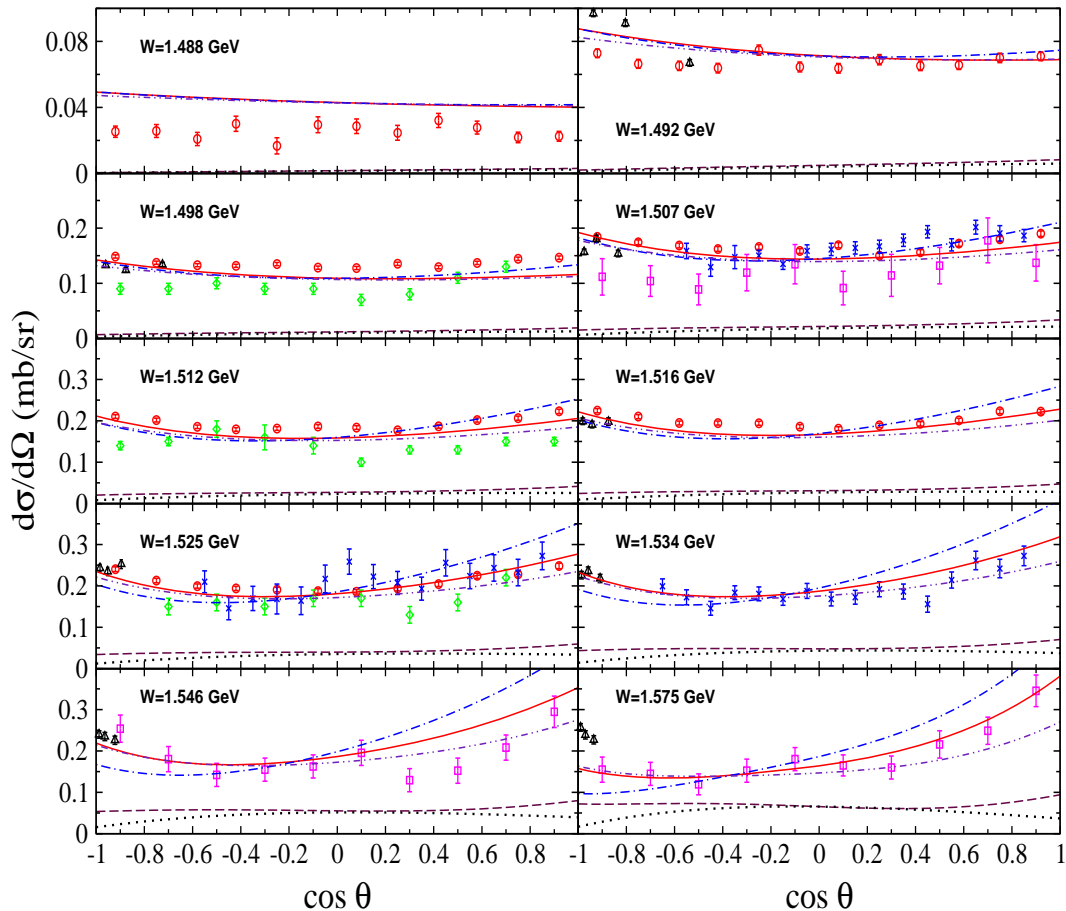
FIG. 5: Differential cross-section for the reaction $\pi^- p \to \eta n$. The full curves correspond to model B and the dotted ones to the non-resonant terms contributions. The other curves have been obtained by removing one resonance from that model; the removed resonances are: $S_{11}(1535)$ (dashed), $P_{11}(1440)$ (dash-dotted), and $P_{13}(1720)$ (dash-dot-dotted). Data are as in Fig. 1.
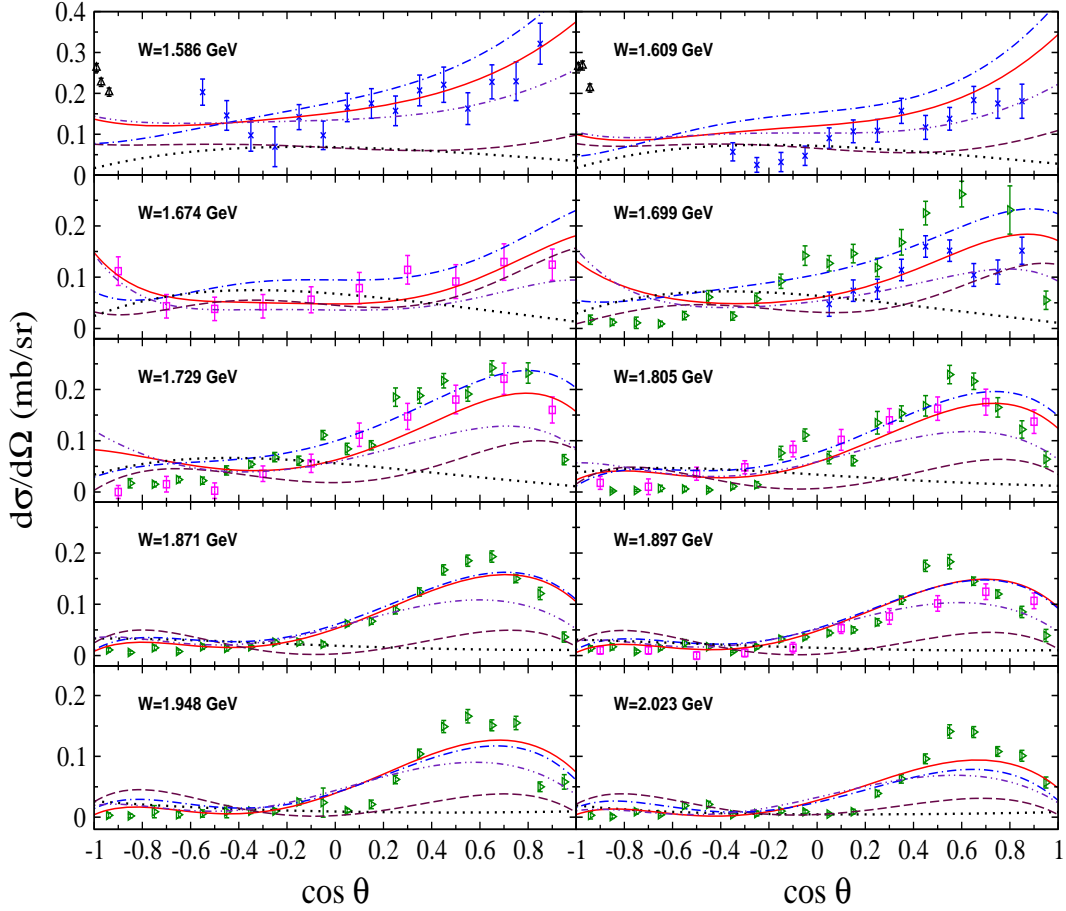
14

FIG. 6: Differential cross-section for the reaction $\pi^- p \to \eta n$. The curves are is in Fig. 5. Data are as in Fig. 2.

As expected, the process is dominated by the $S_{11}(1535)$ resonance. There are however two other resonances playing non-negligible roles, namely, $P_{11}(1440)$ and $P_{13}(1720)$. Figures 5 and 6 show that the importance of those resonances depends on both angle and energy.

The $S_{11}(1535)$ resonance produces more than 80% of the cross-section for the Prakhov *et al.* [28] data. Its importance decreases with energy, especially at backward angles, without vanishing out. The effect of the $P_{11}(1440)$ resonance becomes visible roughly in the energy range $1.525 \leq W \leq 1.8$ GeV, with a destructive behavior at most forward angles. Finally, the $P_{13}(1720)$ appears, in the forward hemisphere, around $W \approx 1.6$ GeV, with the highest contributions at $W \approx 1.73$ GeV and its effect remains constructive.

Although the effect of the $D_{13}(1520)$ on the χ^2 is small, it is required to produce the right

curvature of the curves at low energies.

In conclusion, model B turns out to describe in a satisfactory manner the data set and embodies a simple reaction mechanism. In the following Section we use hence that model for further investigations of the ηN system.

IV.   PREDICTIONS FOR THE ηN SCATTERING LENGTH AND THE $\eta p \to \eta p$ TOTAL CROSS-SECTION

The ηN scattering amplitude in terms of the t-matrix is given by the following relation:

$$f(k) = -\pi \frac{\sqrt{k^2 + m_N^2}\sqrt{k^2 + m_\eta^2}}{\sqrt{k^2 + m_N^2} + \sqrt{k^2 + m_\eta^2}} t_{\eta N}(k, k). \tag{14}$$

Then, the scattering length reads,

$$a_{\eta N} = lim_{k \to 0} f(k). \tag{15}$$

Fig. 7 shows the real and imaginary parts of the function $f(k)$, for model B, and leads to the following value for the scattering length:

$$a_{\eta N} = (0.30 + i0.18) \ fm. \tag{16}$$

Efforts since about two decades to determine the ηN scattering length have recently been reviewed by several authors [40–42]. A lower limit on the imaginary part, derived from the optical theorem and taking into account the recent data [27] leads [42] to 0.172±0.009 fm. Combining results quoted in those review papers, the present knowledge of the imaginary part is:

$$0.17 \ \lesssim \ \mathcal{I}m \ a_{\eta N} \ \lesssim \ 0.49 \ fm, \tag{17}$$

and our value comes out to be within that range.

For the real part of the scattering length the estimates in the literature give [41],

$$0.27 \ \lesssim \ \mathcal{R}e \ a_{\eta N} \ \lesssim \ 1.0 \ fm. \tag{18}$$

The value extracted in the present work, within model B, is close to the lower limit. Our value is compatible with those obtained via chiral effective Lagrangians [43], most recent
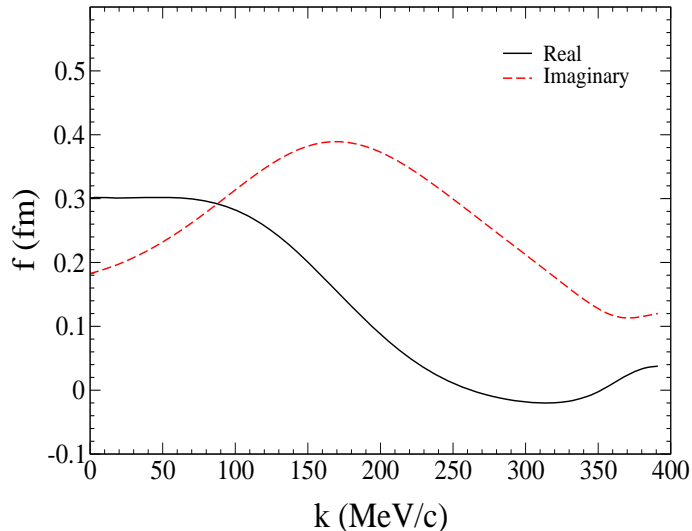
FIG. 7: ηN scattering amplitude $f(k)$ as a function of c.m. momentum, within model B.

solution (G380) from energy-dependent partial-wave analysis [42] of elastic $\pi^\pm p$, $\pi^- p \to \pi^\circ n$, and $\pi^- p \to \eta n$ scattering data, as well as with older findings [44, 45]. Investigations based on chiral perturbation approaches [46, 47] lead to smaller values around 0.2 fm. Finally, coupled-channels calculation within T-matrix [10, 11, 48] or K-matrix [49] produce larger values, $0.5 \lesssim \mathcal{R}e\, a_{\eta N} \lesssim 1.0$ fm.

Besides the process $\pi N \to \eta N$, the η production using proton or deuteron beams have also been investigated using various sets of ηN scattering lengths reported in the literature, as summarized below:

a) $pn \to \eta d$ near threshold data [50] has been studied within a two-step model [45], embodying meson-exchange and final-state ηN interactions, and favors small scattering length: $a_{\eta N} = 0.29 + i0.36$ fm. A microscopic three-body approach in its non-relativistic version [51] reached the conclusion that the data are well reproduced using the results from Ref. [46], $a_{\eta N} = 0.42 + i0.34$ fm. The relativistic version of that approach [52] shows the importance of initial- and final-state treatments, emphasized also by Jülich Group [53], leading to a reduced selectivity on the sets used for the scattering length.

b) $pp \to pp\eta$ [54] and $pn \to pn\eta$ [50] data, as well as the above mentioned data have recently been studied within an effective Lagrangian model [55] resulting in a reasonable

17

account of data for $a_{\eta N} = 0.51 + i0.26$ fm.

c) η production in proton-deuteron collisions are being studied [56], but at the present time those investigations do not allow refinements in determining the ηN scattering length.
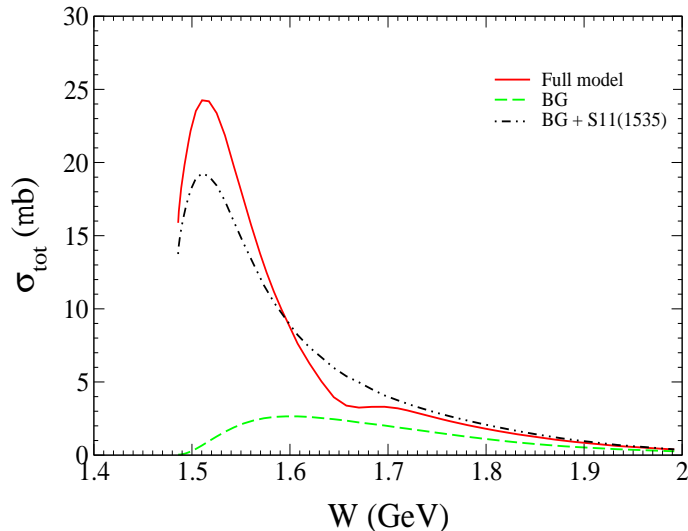

FIG. 8: Total cross-section for the reaction $\eta p \to \eta p$ as a function of total c.m. energy, within model B.

Findings of various approaches with respect to the ηN scattering length, summarized above, lead then to the ranges for real and imaginary parts as reported in Eqs. (17) and (18). Our value for the real part being close to the lower bound, excludes the existence of bound η-nucleus states.

To end this Section, we show our prediction for the ηN elastic scattering total cross-section (Fig. 8). The background contributions (dashed curve) turns out to be small and smoothly varying. This latter contribution completed by that of the $S_{11}(1535)$ (dash-dot-dotted curve) account for a significant portion of the total cross-section predicted by the full model B (full curve).

V. SUMMARY AND CONCLUSIONS

A dynamical coupled-channels formalism is used to study the the process $\pi^- p \to \eta n$ in the total center-of-mass energy range $W \lesssim 2$ GeV. The formalism embodies, besides

non-resonant terms, five intermediate meson-nucleon states, namely, πN, ηN, $\pi \Delta$, σN, and ρN.

Within this phenomenological approach, 34 adjustable parameters are introduced, two of them for the non-resonant mechanisms and the others for the nine nucleon resonances retained in the model search, namely, $S_{11}(1535)$, $S_{11}(1650)$, $P_{11}(1440)$, $P_{11}(1710)$, $P_{13}(1720)$, $D_{13}(1520)$, $D_{13}(1700)$, $D_{15}(1675)$, and $F_{15}(1680)$. That set of resonances corresponds to all known 3 and 4 star resonances relevant to the energy range investigated here.

In order to determine the parameters and build a model, a data set including 294 measured differential cross-sections, coming from five collaborations, are fitted. The selection of data points allows to suppress the manifestations of inconsistencies among available data sets. Our model B reproduces satisfactorily the data, with a reduced $\chi^2 = 1.94$. A detailed study of the reaction mechanism within model B allows to establish a hierarchy in the roles played by nucleon resonances. Actually, the dominant resonance turns out to be the $S_{11}(1535)$. The other resonances affecting the χ^2 by more than 20% when switched off, are by decreasing importance: $P_{11}(1440)$, $P_{13}(1720)$, $S_{11}(1650)$, $F_{15}(1680)$, $P_{11}(1710)$, and $D_{13}(1520)$. Contributions from $D_{13}(1700)$ and $D_{15}(1675)$ are found to be negligible.

Model B is used to extract the ηN scattering length, which comes out to be: $a_{\eta N} = (0.30 + i\,0.18)$ fm. Both the real and imaginary parts of that quantity are within the ranges determined from other works.

To improve our knowledge on the $\pi^- p \rightarrow \eta n$, and consequently on the ηN system, further measurements including polarized target asymmetry, are highly desirable. Such experimental results are awaited for thanks to present and/or forthcoming pion beams in the following labs: GSI [57], ITEP [58], Fermi Lab [59], and JPARC [60].

Finally, to take advantage of copious η electromagnetic production data, the obtained model B appears reliable enough for our in progress investigation of the $\gamma p \rightarrow \eta p$ reaction within a coupled-channels approach and a constituent quark model [61].

---

[1] V. Burkert and T.-S. H. Lee, Int. J. Mod. Phys. E **13**, 1035 (2004).

[2] A. Matsuyama, T. Sato, and T.-S. H. Lee, Phys. Rept. **439**, 193 (2007), and References therein.

[3] Ch. Sauermann, B. L. Friman, and W. Noerenberg, Phys. Lett. **B341**, 261 (1995).

[4] A. M. Green and S. Wycech, Phys. Rev. C **60**, 035208 (1999).

[5] T. Feuster and U. Mosel, Phys. Rev. C **58**, 457 (1998).

[6] G. Penner, PhD Thesis, Universit of Justus-Liebig, Giessen (2002).

[7] G. Penner and U. Mosel, Phys. Rev. C **66**, 055211 (2002).

[8] A. V. Anisovich, A. V. Sarantsev, O. Bartholomy, E. Klempt, V. A. Nikonov, and U. Thoma, Eur. Phys. J. A **25**, 427 (2005).

[9] A. V. Sarantsev, V. A. Nikonov, A. V. Anisovich, E. Klempt, and U. Thoma, Eur. Phys. J. A **25**, 441 (2005).

[10] M. Batinić, I. Šlaus, A. Švarc, and B. M. K. Nefkens Phys. Rev. C **51**, 2310 (1995); Erratum *ibid* **57**, 1004 (1998).

[11] M. Batinić, I. Šlaus, and A. Švarc, Phys. Rev. C **52**, 2188 (1995).

[12] M. Batinić, I. Dadić, I. Šlaus, A. Švarc, B. M. K. Nefkens, and T.-S.H. Lee, arXive: nucl-th/9703023.

[13] S. Ceci, A. Švarc, and B. Zauner, Phys. Rev. Lett. **97**, 062002 (2006).

[14] R. A. Arndt, W. J. Briscoe, I. I. Strakovsky, and R. L. Workman, Phys. Rev. C **74**, 045205 (2006).

[15] B. Juliá-Díaz, T.-S.H. Lee, A. Matsuyama, and T. Sato, Phys. Rev. C **76**, 065201 (2007).

[16] T. Sato and T. S. H. Lee, Phys. Rev. C **54** 2660 (1996).

[17] G.-Y Chen, S. Kamalov, S. N. Yang, D. Drechsel, and L. Tiator, Nucl. Phys. **A723**, 447 (2003).

[18] G.-Y Chen, S.S. Kamalov, S.N. Yang, D. Drechsel, and L. Tiator, Phys. Rev. C **76**, 035206 (2007).

[19] A. M. Gasparyan, J. Haidenbauer, C. Hanhart, and J. Speth, Phys. Rev. C **68**, 045207 (2003).

[20] S. Capstick, T.-S. H. Lee, W. Roberts, and A. Švarc, Phys. Rev. C **59**, R3002 (1999).

[21] X.H. Zhong, Q. Zhao, J. He, and B. Saghai, Phys. Rev. C **76**, 065205 (2007).

[22] B. Saghai, J.-C. David, B. Juliá-Díaz, and T.-S. H. Lee, Eur. Phys. J. A **31**, 512 (2007).

[23] W.-T. Chiang, F. Tabakin, T.-S. H. Lee, and B. Saghai, Phys. Lett. **B517**, 101 (2001).

[24] W.-T. Chiang, B. Saghai, F. Tabakin, and T.-S. H. Lee, Phys. Rev. C **69**, 065208 (2004).

[25] B. Juliá-Díaz, B. Saghai, T.-S. H. Lee, and F. Tabakin, Phys. Rev. C **73**, 055204 (2006).

[26] S. Capstick and W. Roberts, Prog. Part. Nucl. Phys. **45**, 5241 (2000), and references therein.

[27] T. W. Morrison, PhD Thesis, George Washington University, UMI-99-55477 (2000).

[28] S. Prakhov *et al.*, Phys. Rev. C **72**, 015203 (2005).

[29] W. Deinet *et al.*, Nucl. Phys. **B11**, 495 (1969).

[30] W. B. Richards *et al.*, Phys. Rev. D **1**, 10 (1970).

[31] N. C. Debenham *et al.*, Phys. Rev. D **12**, 2545 (1975).

[32] R. M. Brown *et al.*, Nucl. Phys. **B153**, 89 (1979).

[33] R. H. Crouch *et al.*, Phys. Rev. D **21**, 3023 (1980).

[34] J. Feltesse *et al.*, Nucl. Phys. **B93**, 242 (1975).

[35] V. Z. Peterson *et al.*, University of California Radiation Laboratory Report N° UCRL-11576 (1964); F. Bulos *et al.*, Phys. Rev. **187**, 1827 (1969); J. E. Nelson, PhD thesis, Lawrence Berkeley Laboratory Report LBL-1019 (1972); R. B. Chaffee, PhD thesis, Lawrence Berkeley Laboratory Report N° LBL-1060 (1975).

[36] M. Clajus and B. M. K. Nefkens, PiN Newslett. **7**, 76 (1992).

[37] B. Juliá-Díaz, H. Kamano, T.-S.H. Lee, A. Matsuyama, T. Sato, in preparation.

[38] W. M. Yao *et al.*, J. Phys. G **33**, 1 (2006).

[39] CNS Data Analysis Center, GWU, http://gwdac.phys.gwu.edu.

[40] A. Sibirtsev, S. Schneider, Ch. Elster, J. Haidenbauer, S. Krewald, and J. Speth, Phys. Rev. C **65**, 044007 (2002).

[41] A. M. Green and S. Wycech, Phys. Rev. C **71**, 014001 (2005).

[42] R. A. Arndt, W. J. Briscoe, T. W. Morrison, I. I. Strakovsky, and R. L. Workman, Phys. Rev. C **72**, 045202 (2005).

[43] J. Caro Ramon, N. Kaiser, S. Wetzel, and W. Weise, Nucl. Phys. A **672**, 249 (2000).

[44] R. S. Bhalerao and L. C. Liu, Phys. Rev. Lett. **54**, 865 (1985); Q. Haider and L. C. Liu, Phys. Lett. **B172**, 257 (1986); C. Bennhold and H. Tanabe, Nucl. Phys. **A530**, 625 (1991).

[45] V. Yu. Grishina, L. A. Kondratyk, M. Buscher, C. Hanhart, J. Haidenbauer, and J. Speth, Phys. Lett. **B475**, 9 (2000).

[46] N. Kaiser, T. Waas, and W. Weise, Nucl. Phys. **A612**, 297 (1997).

[47] Yan-Rui Liu and Shi-Lin Zhu, Phys. Rev. C **75**, 034003 (2007).

[48] M. Arima, K. Shimizu, and K. Yazaki, Nucl. Phys. **A543**, 613 (1992); V. V. Abaev and B. M. K. Nefkens, Phys. Rev. C **53**, 385 (1996); M. Batinic, I. Slaus, A. Švarc, B. M. K. Nefkens, and T.-S. H. Lee, Phys. Scr. **58**, 15 (1998); O. Krehl, C. Hanhart, S. Krewald, and J. Speth, Phys. Rev. C **62**, 025207 (2000).

[49] Ch. Deutsch-Sauermann, B.L. Friman, and W. Nrenberg, Phys. Lett. B **409**, 51 (1997); A.M. Green and S. Wycech, Phys. Rev. C **55**, R2167 (1997); A.M. Green and S. Wycech, Phys. Rev. C **60**, 035208 (1999).

[50] H. Calen *et al.*, Phys. Rev. Lett. **79**, 2642 (1997); *ibid* **80**, 2069 (1998).

[51] H. Garcilazo and M. T. Peña, Phys. Rev. C **66**, 034606 (2002).

[52] H. Garcilazo and M.T. Peña, Phys. Rev. C **72**, 014003 (2005).

[53] V. Baru, A. M. Gasparyan, J. Haidenbauer, C. Hanhart, A. E. Kudryavtsev, and J. Speth, Phys. Rev. C **67**, 024002 (2003).

[54] P. Moskal *et al.*, Phys. Rev. C **69**, 025203 (2004), and references therein.

[55] R. Shyam, Phys. Rev. C **75**, 055201 (2007).

[56] H.-H. Adam *et al.*, Phys. Rev. C **75**, 014004 (2007); J. Smyrski *et al.*, Phys. Lett. **B649**, 258 (2007); N. J. Upadhyay, K. P. Khemchandani, B. K. Jain, and N. G. Kelkar, Phys. Rev. C **75**, 054002 (2007); K. P. Khemchandani, N. G. Kelkar, and B. K. Jain, *ibid* **76**, 069801 (2007).

[57] M. L. Benabderrahmane (for the FOPI Collaboration), Acta. Phys. Polon. B **37**, 167 (2006).

[58] I. G. Alekseev *et al.* (EPECUR and ITEP-PNPI Collaborations), arXiv: hep-ex/0509032.

[59] R. Raja, arXiv: hep-ex/0612007.

[60] *see e.g.* J. Imazato, Nucl. Phys. Proc. Suppl. **129**, 81 (2004).

[61] B. Saghai and Z. Li, Eur. Phys. J. A **11**, 217 (2001); J. He, B. Saghai, Z. Li, Q. Zhao, and J. Durand, Eur. Phys. J. A **35**, 321 (2008); J. He, B. Saghai, and Z. Li, arXiv: 0802.3816 [nucl-th].